Journal of Rock Mechanics and Geotechnical Engineering 16 (2024) 1113–1126

Contents lists available at ScienceDirect

Journal of Rock Mechanics and Geotechnical Engineering

journal homepage: www.jrmge.cn

Full Length Article

Evolution of mechanical parameters of Shuangjiangkou granite under different loading cycles and stress paths

Liangjie Gu [a], Xia-Ting Feng [a,*], Rui Kong [a,**], Chengxiang Yang [a], Yuelin Xia [b]

[a] Key Laboratory of Ministry of Education on Safe Mining of Deep Metal Mines, Northeastern University, Shenyang, 110819, China
[b] State Key Laboratory of Geomechanics and Geotechnical Engineering, Institute of Rock and Soil Mechanics, Chinese Academy of Sciences, Wuhan, 430071, China

ARTICLE INFO

Article history:
Received 19 February 2023
Received in revised form
1 July 2023
Accepted 4 September 2023
Available online 25 October 2023

Keywords:
Triaxial cyclic loading and unloading test
Stress path
Deformation modulus and elastic deformation increment ratios
Fracture degree
Cohesion and internal friction angle

ABSTRACT

Surrounding rocks at different locations are generally subjected to different stress paths during the process of deep hard rock excavation. In this study, to reveal the mechanical parameters of deep surrounding rock under different stress paths, a new cyclic loading and unloading test method for controlled true triaxial loading and unloading and principal stress direction interchange was proposed, and the evolution of mechanical parameters of Shuangjiangkou granite under different stress paths was studied, including the deformation modulus, elastic deformation increment ratios, fracture degree, cohesion and internal friction angle. Additionally, stress path coefficient was defined to characterize different stress paths, and the functional relationships among the stress path coefficient, rock fracture degree difference coefficient, cohesion and internal friction angle were obtained. The results show that during the true triaxial cyclic loading and unloading process, the deformation modulus and cohesion gradually decrease, while the internal friction angle gradually increases with increasing equivalent crack strain. The stress path coefficient is exponentially related to the rock fracture degree difference coefficient. As the stress path coefficient increases, the degrees of cohesion weakening and internal friction angle strengthening decrease linearly. During cyclic loading and unloading under true triaxial principal stress direction interchange, the direction of crack development changes, and the deformation modulus increases, while the cohesion and internal friction angle decrease slightly, indicating that the principal stress direction interchange has a strengthening effect on the surrounding rocks. Finally, the influences of the principal stress interchange direction on the stabilities of deep engineering excavation projects are discussed.

1. Introduction

Surrounding rocks at different locations are generally subjected to different stress paths during the process of deep hard rock excavation (Eberhardt, 2001; Chen and Huang, 2007; Andersson et al., 2009; Bai et al., 2019; Jiang et al., 2019), which often induces brittle disasters, such as rockbursts, spalling and collapse (Ortlepp, 2005; Martin and Christiansson, 2009; Li et al., 2009; Feng, 2017; Duan et al., 2019; Zhao et al., 2022), and significantly affects the progress of construction and the safety of personnel. The process of brittle failure of surrounding rocks includes the initiation, propagation and coalescence of microcracks under different stress paths (Kaiser, 2005; Diederichs, 2007; Heap and Faulkner, 2008; Rojat et al., 2009; Huang and Huang, 2014; Chen et al., 2016; Liang et al., 2017; Renani and Martin, 2018; Kong et al., 2021; Zhang et al., 2021; Zhu et al., 2022). However, the final failure state provides limited information and the failure process of rocks cannot be accurately described. Therefore, it is important to accurately understand the evolution of rock mechanical parameters under different stress paths for revealing the mechanics underpinning rock mass instability. For this reason, the cyclic loading and unloading tests have been widely conducted (Renani and Martin, 2018; Wang et al., 2019a; Meng et al., 2021; Zhou et al., 2022; Jiang et al., 2023; Liu et al., 2023a).

Cyclic loading and unloading tests are efficient methods to study and quantitatively describe the deformation and fracture behavior of rocks in different stress states. Many scholars have theoretically investigated the fracture characteristics and mechanical properties of rocks by conducting uniaxial and conventional triaxial cyclic

* Corresponding author.
** Corresponding author.
E-mail addresses: fengxiating@mail.neu.edu.cn (X.-T. Feng), kongrui@mail.neu.edu.cn (R. Kong).

Peer review under responsibility of Institute of Rock and Soil Mechanics, Chinese Academy of Sciences.

https://doi.org/10.1016/j.jrmge.2023.09.005

loading tests (Martin and Chandler, 1994; Poinard et al., 2010; Xiao et al., 2010; Momeni et al., 2015; Zhao et al., 2017; Yin et al., 2023). Examples include the relationships of Young's modulus, Poisson's ratio and plastic strain (Taheri et al., 2016; Duan et al., 2021a) with nonlinear characteristics of deformation considering the influences of confining pressure on the dilatancy angle and plastic strain (Heap and Faulkner, 2008; Qiu et al., 2014). For example, Cai et al. (2023) developed a mechanical model of the dilation angle, which can better simulate nonlinear post-peak mechanical behavior. Additionally, the evolutions of cohesion and the internal friction angle of rocks under cyclic loading and unloading conditions are obtained by analyzing the propagation of microcracks, fractures and strength criteria and establishing corresponding constitutive models (Hoek and Brown, 1997; Hajiabdolmajid et al., 2002; Sun et al., 2017; Feng et al., 2021). It is worth noting that the underground excavation environment is in a true three-dimensional (3D) stress state (Cai et al., 2004; Lee and Haimson, 2011), and thus the true triaxial cyclic loading and unloading tests have been conducted to investigate the evolution of the deformation, strength and energy of rocks. The results show that fracture development in rocks is anisotropic under the influence of intermediate principal stress (Feng et al., 2020a; Duan et al., 2021b; Liu et al., 2023b).

However, most of the above tests were designed for such loading conditions in which σ_2 and σ_3 are set to constant values. In practice, the fracture evolution of rock under loading conditions mentioned above is different from that during excavation in which σ_3 decreases and σ_2 is adjusted (Eberhardt, 2001; Jiang et al., 2019; Bai et al., 2019; Gu et al., 2022), and thus there are also differences in the evolution of fracture mechanism of rock masses for loading-unloading stress paths during excavation (Huang et al., 2001; Li et al., 2017a; Feng et al., 2020c). In addition, during excavation, the adjustment of principal stress includes changes in both principal stress magnitude and direction. The phenomenon of changes in stress direction prevails in underground engineering excavation (Kaiser et al., 2001; Diederichs et al., 2004; Zhang et al., 2012; Li et al., 2015; He et al., 2021), which affects the deformation and fracture of rocks (Eberhardt, 2001; Basarir et al., 2015; Li et al., 2017b; Wang et al., 2018, 2019b; Feng et al., 2022; Cai et al., 2022; Gu et al., 2023). Therefore, it is essential to design a reasonable test method for cyclic loading and unloading to investigate the evolution of the mechanical parameters of rocks under different stress paths that occurs during underground engineering.

In this study, using true triaxial test equipment of rocks, the true triaxial cyclic loading and unloading tests are designed and conducted on the granite sampled from the underground powerhouse of the Shuangjiangkou Hydropower Station in China. The evolutions of rock deformation, fracture and strength parameters of rocks under different stress paths are revealed. This study has important theoretical significance and provides valuable engineering guidance for the analysis of rock failure mechanisms and the control of the stability of surrounding rocks in deep excavation projects.

2. Rock specimens and test methods

2.1. Rock specimens

In this study, the porphyritic K-feldspar granite sample was taken from the underground powerhouse of the Shuangjiangkou Hydropower Station in the upper reaches of the Dadu River in Sichuan Province, China. A standard cuboid sample of 50 mm × 50 mm × 100 mm was prepared according to the ISRM suggested method (Feng et al., 2019). The contents of mineral grains including quartz, feldspar, mica are 26.5%, 56%, and 15%, respectively, and the total content of other substances is 2.5%. The wave velocity is approximately 3900 m/s, and the density is approximately 2.68 g/cm^3. The uniaxial compressive strength of the granite is 170 MPa (Gu et al., 2022).

2.2. Test apparatus

In this study, the hard rocks were tested using a high-pressure true triaxial full stress–strain method and a test device that was developed independently at Northeastern University. The apparatus had excellent technical features such as very stiff servo frame loading, adaptive coordinated feedback control, and accurate measurements of fracture and deformation. It has been successful used for full stress–strain tests, true triaxial loading and unloading tests, and tests of principal stress direction interchange of hard rocks under true triaxial compression (Feng et al., 2016).

2.3. Test methodology

Gu et al. (2022) summarized the stress paths at different locations around a deep hard rock excavation. In the high-risk failure zone, the maximum and minimum principal stresses increase and decrease, respectively, and the intermediate principal stress has three forms of slightly increase, constant and decrease. In the medium-risk zone, the maximum principal stress is basically constant, and the variations of the intermediate principal stress and minimum principal stress are the same as those in the high-risk zone. In the low-risk zone, the maximum principal stress decreases, and the variations of the intermediate principal stress and minimum principal stress are also similar to those in the high-risk zone. The surrounding rocks near the excavation sidewall bear different loading and unloading stress paths. With the advance of the working face, the stress concentration area moves deeper inside surrounding rocks, which can usually bear the loading stress path. Furthermore, in deep excavation, both the stress magnitude and direction change. Gu et al. (2023) provided two case studies of intermediate principal stress and maximum principal stress direction interchange, which showed the effect of intermediate principal stress and maximum principal stress direction interchange on failure behavior of rocks. Therefore, in this study, three cyclic loading and unloading control methods were designed to explore the evolution of the mechanical parameters of rocks under different stress paths. The specific control methods are described as follows.

2.3.1. Cyclic loading and unloading under true triaxial loading and unloading (CLU–TLU)

Due to the failure of surrounding rocks near the sidewall during loading and unloading stress paths after underground excavation, a new cyclic loading and unloading control method under true triaxial conditions was designed (Fig. 1a) to measure the evolution of the mechanical parameters of rocks during true triaxial cyclic loading and unloading. The specific test steps are as follows:

(i) Step 1: Initial stress loading stage. First, the σ_1, σ_2 and σ_3 were loaded simultaneously at a rate of 0.5 MPa/s to reach the predefined value of σ_3, while σ_3 was kept constant. Then, σ_1 and σ_2 were loaded simultaneously at a rate of 0.5 MPa/s to reach the predefined value of σ_2, while σ_2 was kept constant. Finally, σ_1 was loaded at a rate of 0.5 MPa/s to 80% of peak strength of rocks (σ_p) to ensure that rocks can be fractured before σ_3 was unloaded to 0. To obtain 80% of peak strength of rocks, the in situ stresses $\sigma_2 = 20$ MPa and $\sigma_3 = 10$ MPa for the Shuangjiangkou underground powerhouse were used as the basis. Three repetitions of the true triaxial compression test were performed with stress levels of $\sigma_2 = 20$ MPa and

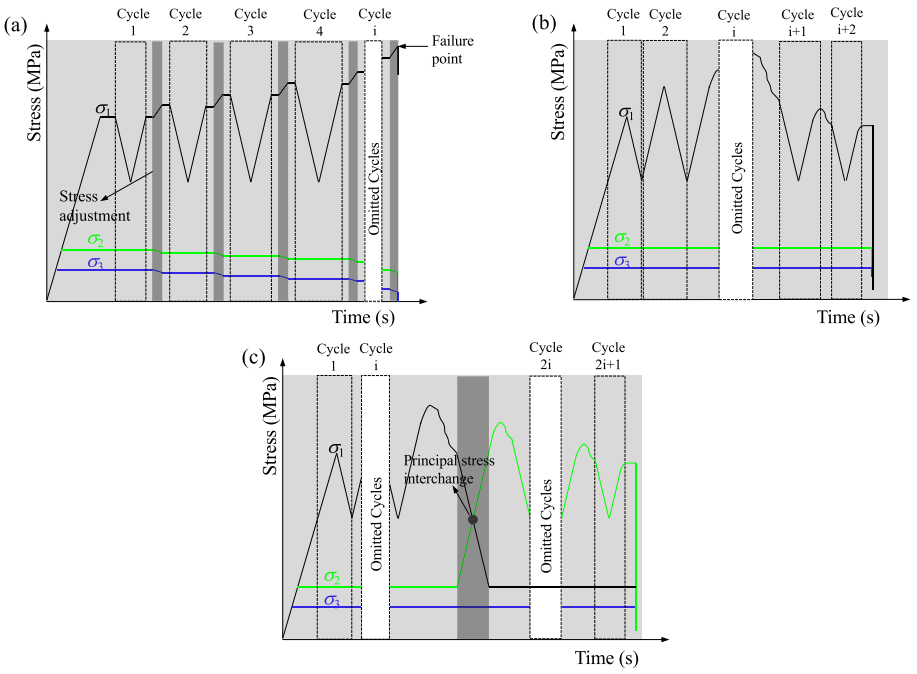

Fig. 1. Schematic diagrams of stress paths: (a) Cyclic loading and unloading under true triaxial loading and unloading, (b) Cyclic loading and unloading under true triaxial compression, and (c) Cyclic loading and unloading under true triaxial principal stress direction interchange.

$\sigma_3 = 10$ MPa. The variation of the peak strengths of the three groups was less than 1.5%, with the average peak strength of 299 MPa. Overall, 80% of the peak strengths were 238 MPa.

(ii) Step 2: Cyclic loading and unloading stage. At this stage, the σ_2 and σ_3 remained constant, and σ_1 increased and decreased at a rate of 0.5 MPa/s. The final σ_1 was unloaded to 30 MPa greater than the initial predefined σ_2.

(iii) Step 3: Stress adjustment stage. According to the predefined stress path, the three principal stresses were adjusted at their respective rates, in which the loading rate of σ_1 was 0.06 MPa/s, the loading and unloading rates of σ_2 were 0.01 MPa/s, and the unloading rate of σ_3 was 0.02 MPa/s. After stress adjustment, the three principal stresses were kept stable for approximately 1–2 min. When the stress state was stable, the next cycle was performed until the specimen fractured.

2.3.2. Cyclic loading and unloading under true triaxial compression (CLU–TC)

The deep surrounding rocks usually show a loading stress path. The cyclic loading and unloading control method was adopted (Fig. 1b) to obtain the evolution of the mechanical parameters of rock under true triaxial compression loading. The specific test steps are as follows:

(i) Step 1: Initial stress loading stage. The steps for loading σ_2 and σ_3 to the initial stress level were the same as those of the CLU–TLU. It is worth noting that when the deformation rate in σ_3 direction was approximately 0.015 mm/min, the loading of σ_1 was servo-controlled to facilitate the acquisition of the post-peak stage.

(ii) Step 2: Cycle loading and unloading stage. At this stage, σ_1 increased and decreased in cycles at rates of 0.5 MPa/s, during which σ_2 and σ_3 remained constant; the final σ_1 was unloaded to 10 MPa greater than the initial predefined σ_2. Then, the next cycle was performed successively until the sample reached the residual stage. In this test, σ_1 was unloaded to the initial predefined σ_2 value that exceeded 10 MPa to prevent the value of σ_1 after unloading from being less than the residual strength.

2.3.3. Cyclic loading and unloading under true triaxial principal stress direction interchange (CLU–TSI)

Since underground excavation includes adjusting the stress direction, a new cyclic loading and unloading control method under true triaxial principal stress direction interchange was designed (Fig. 1c) to obtain the evolution of the mechanical parameters of rocks under the direction interchange of true triaxial principal stress. The specific test steps are as follows:

(i) Step 1: Initial stress loading stage. This stage was consistent with CLU–TC testing.

(ii) Step 2: Cyclic loading and unloading stage. This stage was consistent with CLU–TLU testing.

(iii) Step 3: Principal stress direction interchange stage.

When reaching the interchange point between σ_2 and σ_1 directions, σ_1 is decreased at a rate of 1 MPa/s, while σ_2 is increased at a rate of 0.5 MPa/s to prevent the sudden failure of rocks during the interchange of principal stress directions, until σ_1 decreased to the σ_2 level and then remained constant. σ_2 interchanged to σ_1, and cyclic loading and unloading continued. During the increase in intermediate principal stress, the ε_3 deformation rate was kept constant near 0.015 mm/min. Then, the next cycle was applied until the sample reached the residual stage.

Notably, the rate of 0.5 MPa/s used for loading is suggested by ISRM (Kovari et al., 1983). For the loading and unloading processes, considering the stress path, the rates of σ_1, σ_2 and σ_3 were 0.06 MPa/

Table 1
Testing schemes and results.

Test type	No.	σ_3^0 (MPa)	σ_2^0 (MPa)	σ_1^0 (MPa)	σ_3^f (MPa)	σ_2^f (MPa)	σ_1^f (MPa)	p^f	q^f	Cycles	Corresponding simple stress path
CLU–TLU	SKJ-1-1	10	20	238	0	20	228	83	219	10	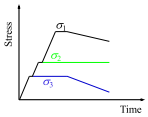
	SKJ-1-2	10	20	238	3	20	238	87	227	7	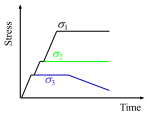
	SKJ-1-3	10	20	238	5.95	20	250	92	237	5	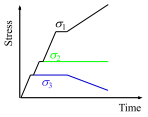
	SKJ-1-4	10	20	238	2	28	262	97	248	8	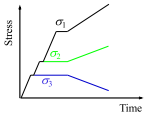
	SKJ-1-5	10	20	238	5	15	253	91	243	5	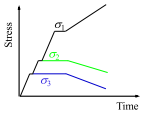
CLU–TC	SKJ-1-6	10	20		10	20	310	113	295	14	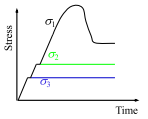
CLU–TSI	SKJ-1-7	10	20		10	20	292	107	277	12	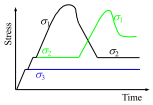

s, 0.01 MPa/s, and 0.02 MPa/s, respectively, since the unloading rate should meet the strain rate requirements ranging from 10^{-6} s^{-1} to 10^{-2} s^{-1} (Kovari et al., 1983). Additionally, the unloading rate adopted in this study was well within the range of unfavorable unloading rates (Qiu et al., 2014; Xu et al., 2019), and thus the loading and unloading rates were finally determined for the convenience of test control by fully considering the above two reasons.

The specific test scheme and results are shown in Table 1, where σ_1^0, σ_2^0 and σ_3^0 are the initial stress states in the σ_1, σ_2 and σ_3 directions, respectively; σ_1^f, σ_2^f and σ_3^f are the peak stress states in the σ_1, σ_2 and σ_3 directions, respectively; and p^f and q^f are the peak generalized shear stress and the peak average stress, respectively.

3. Deformation and fracture parameters

3.1. Stress–strain curves

Fig. 2 shows the typical stress–strain curves of Shuangjiangkou granite during cyclic loading and unloading under different stress paths. It can be found that the ε_1 at the peak point of each cycle gradually increased in the positive direction and showed compression characteristics, while the ε_2 and ε_3 developed in the negative direction and showed expansion characteristics. In the CLU–TSI test, due to the direction interchange of σ_1 and σ_2, the deformation in the initial maximum principal stress direction changed from compression to expansion, and the deformation in the initial intermediate principal stress direction changed from expansion to compression (Fig. 2g).

3.2. Deformation parameters

In this study, the deformation modulus and elastic deformation increment ratios of Shuangjiangkou granite during cyclic loading and unloading under different stress paths are calculated, as expressed in Eqs. (1)–(3). Due to the effect of true triaxial stress, the values of the elastic deformation increment ratios in the σ_3 and σ_2 directions are different.

$$E_1 = \frac{\mathrm{d}\sigma_1}{\mathrm{d}\varepsilon_1^e} \tag{1}$$

$$\nu_{12} = \frac{\mathrm{d}\varepsilon_2^e}{\mathrm{d}\varepsilon_1^e} \tag{2}$$

$$\nu_{13} = \frac{\mathrm{d}\varepsilon_3^e}{\mathrm{d}\varepsilon_1^e} \tag{3}$$

where E_1 is the deformation modulus in the σ_1 direction; ν_{12} and ν_{13} are the elastic deformation increment ratios in the σ_2 and σ_3 directions, respectively; and $\mathrm{d}\varepsilon_1^e$, $\mathrm{d}\varepsilon_2^e$ and $\mathrm{d}\varepsilon_3^e$ are the elastic strain increments in the σ_1, σ_2 and σ_3 directions, respectively. In addition,

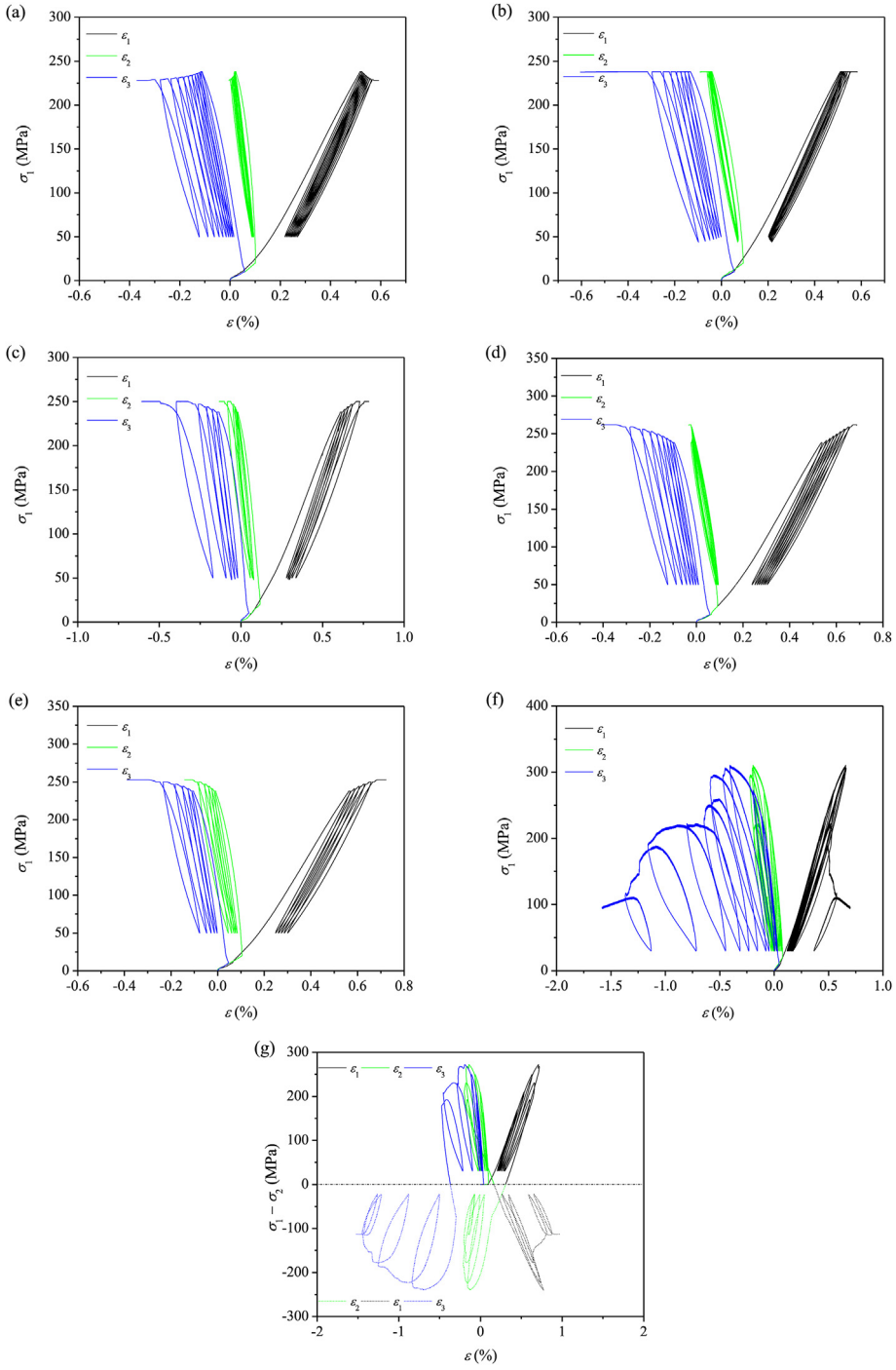

Fig. 2. Typical stress–strain curves of Shuangjiangkou granite during cyclic loading and unloading under different stress paths: (a) SKJ-1-1, (b) SKJ-1-2, (c) SKJ-1-3, (d) SKJ-1-4, (e) SKJ-1-5, (f) SKJ-1-6, and (g) SKJ-1-7.

the elastic parameters of rocks are analyzed according to the elastoplastic theory. It is considered that elastic parameters are affected by plasticity and damage. When the specimen is failed, the strain is no longer uniform, and the equivalent strain is used to describe the overall law.

The deformation of rock is divided into elastic strain and crack-induced deformation. The elastic strain is recoverable, and the crack-induced deformation is irreversible strain, which represents the fracture characteristics of rocks. The equivalent crack strain caused by three principal stress directions is used to characterize the fracture evolution process of rocks. The equivalent crack strain is written as

$$\overline{e^{\mathrm{p}}} = \sum \sqrt{\left(\mathrm{d}\varepsilon_1^{\mathrm{p}}\right)^2 + \left(\mathrm{d}\varepsilon_2^{\mathrm{p}}\right)^2 + \left(\mathrm{d}\varepsilon_3^{\mathrm{p}}\right)^2} \tag{4}$$

where $\overline{e^{\mathrm{p}}}$ is the equivalent crack strain; and $\mathrm{d}\varepsilon_1^{\mathrm{p}}$, $\mathrm{d}\varepsilon_2^{\mathrm{p}}$ and $\mathrm{d}\varepsilon_3^{\mathrm{p}}$ are the crack strain increments in the σ_1, σ_2 and σ_3 directions, respectively.

Due to the stress control mode used in the CLU–TLU test, the rock sample failed rapidly once the stress reached peak strength at

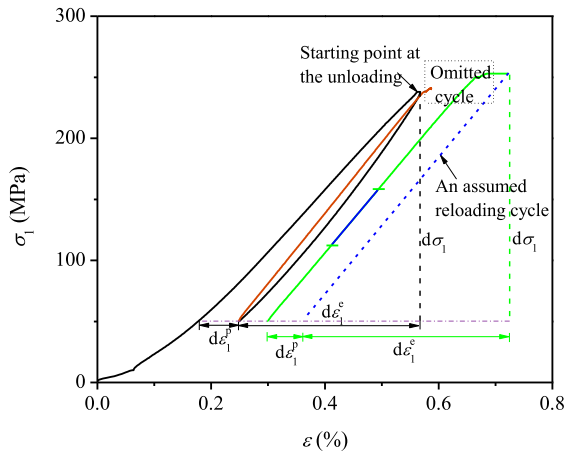

Fig. 3. Method for evaluating the deformation modulus under the ultimate load using a hypothetical reloading and unloading cycle.

constant loading and unloading rates, and the unloading displacement at the final failure was not measured. Therefore, it was assumed that the deformation modulus under the ultimate load was the same as that of the loading section in the last cycle. As shown in Fig. 3, the slope of the dotted line below the axial strain curve was the same as that of loading at this cyclic stage. This assumption was based on the idea that the values of the deformation modulus during loading and unloading were approximately identical, which exerts little influence on the overall evolution of rock fracture.

Fig. 4 shows the evolutions of the deformation modulus and elastic deformation increment ratios with equivalent crack strain during the processes of cyclic loading and unloading on Shuangjiangkou granite under different stress paths. It can be found that the deformation modulus of tested rocks gradually decreased in the CLU–TLU test, which decreased to the minimum value when the rock's ultimate bearing capacity was reached. For the CLU–TC test, the deformation modulus of rocks was greatly reduced when the peak strength was reached, and then decreased gradually at the post-peak stage.

The evolution of the elastic deformation increment ratios is different due to the adjustment trends of the three principal stresses, especially the adjustment of σ_2, which greatly influenced ν_{12} and ν_{13}. In the CLU–TLU test, the stress adjustment trends of σ_1 and σ_3 were maintained. When σ_2 was loaded, ν_{12} gradually decreased, and ν_{13} continuously increased (Fig. 4d). When σ_2 was constant and unloaded, ν_{12} and ν_{13} increased continuously, but the growth trend of ν_{12} at σ_2 unloading exceeded the stress path at constant σ_2 (Fig. 4c and e).

In the CLU–TSI test, the deformation modulus decreased while the elastic deformation increment ratios increased at the initial stage. With the interchange of the σ_2 and σ_1 directions, the deformation modulus increased, while the values of ν_{12} and ν_{13} decreased (Fig. 4g), indicating that the ability of rocks to resist deformation increased after the interchange of the principal stress directions. This is because the development of damage and fracture is parallel to the intermediate principal stress direction under true triaxial conditions. After the interchange of the intermediate and maximum principal stresses, the direction of damage and fracture development will deviate. As a result, rocks will not deteriorate along the original damage direction, but will develop along the new damage direction. Meanwhile, the degree of damage in the new direction is smaller than that in the original development area, and thus rocks will have a certain strengthening effect (Gu et al., 2023), resulting in an increase in the deformation modulus.

3.3. Fracture parameters

Fig. 5 shows the typical macroscopic failure mode of Shuangjiangkou granite during cyclic loading and unloading under different stress paths. It can be found that rock fracture was parallel to the direction of the intermediate principal stress under true triaxial conditions, while the fracture angle was different under various stress paths (Fig. 5a–e). To better compare the failure angles under different stress paths, the failure angle is defined as the angle between the failure surface and the initial maximum principal stress loading surface. Although this is a two-dimensional failure angle, it can to some extent illustrate the failure characteristics of rocks. When σ_3 was smaller or the stress difference $\sigma_2-\sigma_3$ was larger at rock failure, the fracture angle of rocks was larger, which was shown as splitting failure (Fig. 5a and d). In the CLU–TSI test, due to the interchange of the σ_1 and σ_2 directions, the macroscopic failure surfaces were cross-connected, and the failure angles in the σ_1 and σ_2 directions are 90° and 72°, respectively (Fig. 5g). This behavior occurred because the fracture development was parallel to the σ_2 direction under the true triaxial condition. Due to the direction interchange between the maximum and intermediate principal stresses, the direction of crack development changed, which changed the difference characteristics of fracture.

To further describe the fracture evolution of rocks under different stress paths, the deformation caused by cracks was used to represent the fracture characteristics of rocks, and the proportion of strain caused by cracks in the total strain was defined as the fracture degree of rocks. In a physical sense, the fracture degree coefficient is the same as the damage degree of rocks, as expressed in Eqs. (5) and (6):

$$\eta = \frac{d\varepsilon^p}{d\varepsilon} \tag{5}$$

$$d\varepsilon = d\varepsilon^p + d\varepsilon^e \tag{6}$$

where η is the fracture degree coefficient of rocks, $d\varepsilon^p$ is the crack strain increment, and $d\varepsilon$ is the total strain increment. The fracture degree coefficients in the σ_1, σ_2 and σ_3 directions are expressed in Eqs. (7)–(9):

$$\eta_1 = \frac{d\varepsilon_1^p}{d\varepsilon_1} \tag{7}$$

$$\eta_2 = \frac{d\varepsilon_2^p}{d\varepsilon_2} \tag{8}$$

$$\eta_3 = \frac{d\varepsilon_3^p}{d\varepsilon_3} \tag{9}$$

Fig. 6 shows the evolution of the fracture degree of Shuangjiangkou granite in the three principal stress directions with the equivalent crack strain under different stress paths. The overall fracture degree in the three directions was $\eta_1<\eta_2<\eta_3$.

In the CLU–TLU test, when the stress adjustments of σ_2 and σ_3 were consistent, σ_1 increased gradually in the stress path from σ_1 unloading to loading. In the stress path of σ_1 unloading, η_1 remained almost 0 at the initial stage and reached a maximum value of 0.09 when the stress reached its peak strength (Fig. 6a). In the stress path where σ_1 was constant, η_1 increased slowly and reached a maximum value of 0.12 when the stress reached the peak

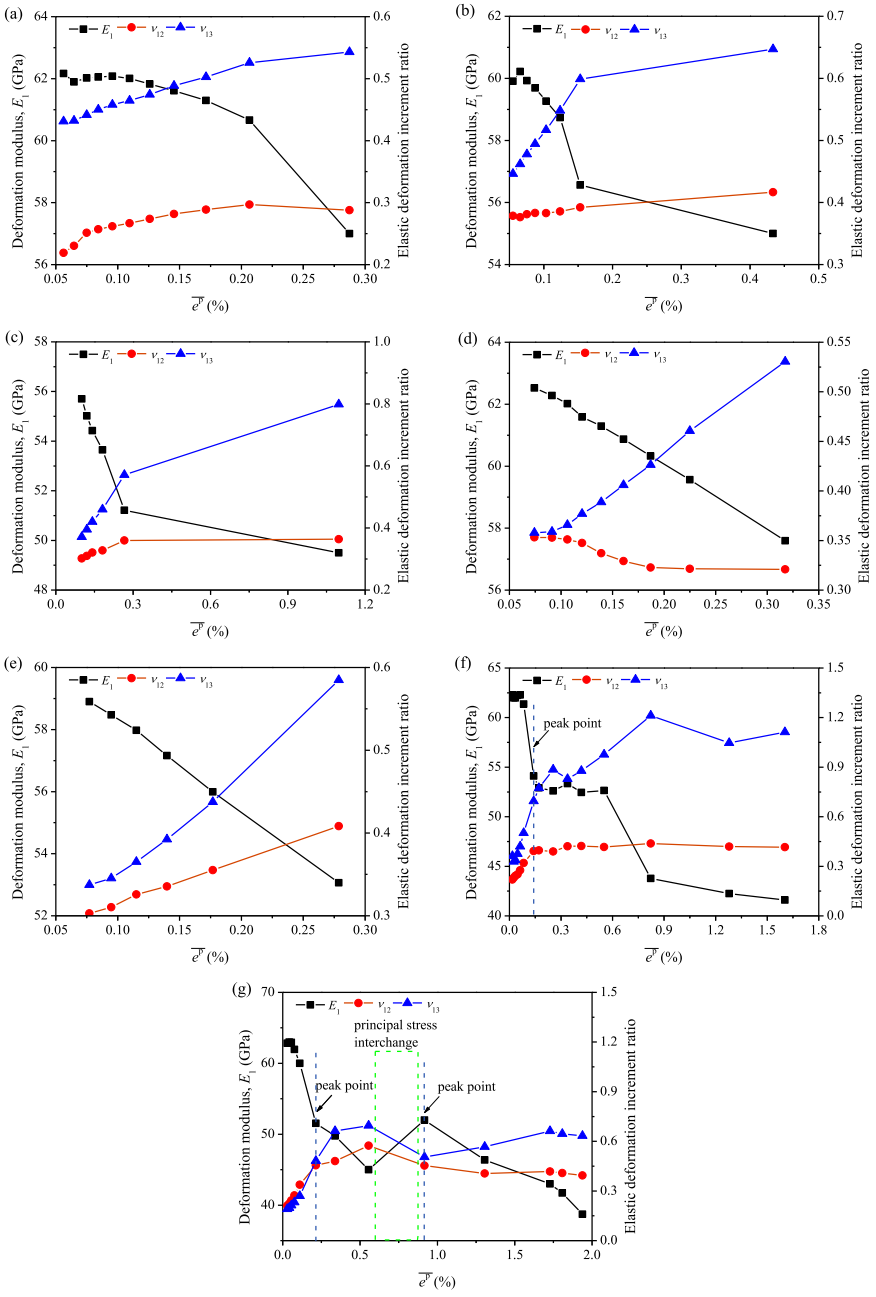

Fig. 4. Evolution of the deformation modulus and elastic deformation increment ratios with equivalent crack strain during cyclic loading and unloading of Shuangjiangkou granite under different stress paths: (a) SKJ-1-1, (b) SKJ-1-2, (c) SKJ-1-3, (d) SKJ-1-4, (e) SKJ-1-5, (f) SKJ-1-6, and (g) SKJ-1-7.

strength (Fig. 6b). In the stress path of σ_1 loading, the upward trend of η_1 increased and reached a maximum value of 0.2 when the stress reached the peak strength (Fig. 6c). Therefore, the increase in σ_1 improved the fracture degree of rocks in the direction of the maximum principal stress. When the stress adjustments of σ_1 and σ_3 were consistent, η_2 gradually decreased in the stress path as σ_2 transitioned from unloading to constant to loading conditions (Fig. 6e, c and d). Therefore, the increase in σ_2 reduced the fracture degree of rocks in the direction of intermediate principal stress.

As shown in Fig. 6f and g, when the peak strength of the rock was reached, the fracture difference in the three principal stress directions was significant in the CLU–TC and CLU–TSI tests. The fracture degree in the σ_3 direction was much larger than that in the σ_2 and σ_1 directions. At the post-peak stage, the fracture degree of σ_3 was still maintained at a high level, indicating that the fracture was mainly parallel to the direction of σ_2 under true triaxial conditions, which showed characteristics of fracture difference. In the CLU–TSI test, when the σ_2 and σ_1 directions were interchanged, the fracture degrees in the three principal stress directions decreased. This result occurred because the direction of crack generation changed after the direction of the principal stress interchanged. The fracture degree of the location decreased where the new crack generated, reducing the fracture degrees in the three directions. Additionally, due to the interchanges in the σ_1 and σ_2 directions, the growth rate of η_1 accelerated, and the growth rate of η_2 decelerated.

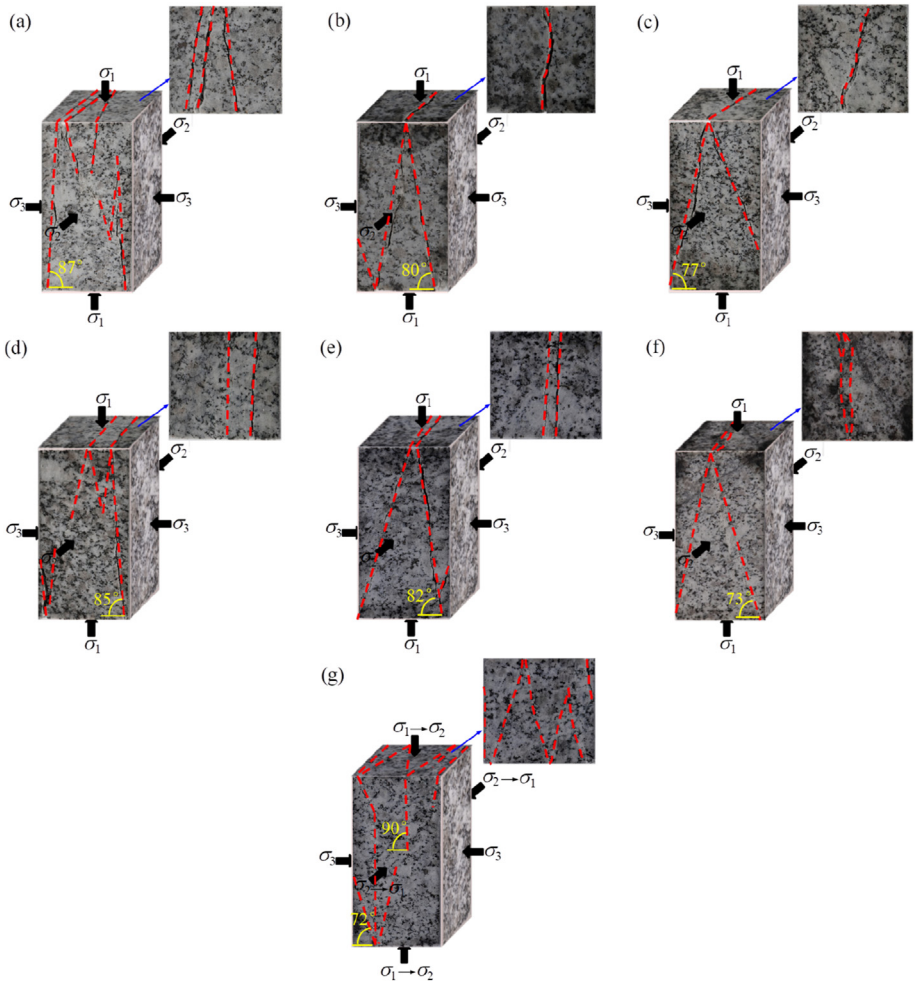

Fig. 5. Macroscopic failure mode of Shuangjiangkou granite during cyclic loading and unloading under different excavation stress paths: (a) SKJ-1-1, (b) SKJ-1-2, (c) SKJ-1-3, (d) SKJ-1-4, (e) SKJ-1-5, (f) SKJ-1-6, and (g) SKJ-1-7.

4. Strength parameters

4.1. Methods for determining the cohesion and internal friction angle

As two basic strength parameters of rocks, the cohesion (c) and internal friction angle (φ) were calculated by Renani and Martin (2018) using the Mohr–Coulomb criterion through a conventional triaxial cyclic loading and unloading test. Because rocks are in a true triaxial stress environment and affected by excavation, the surrounding rocks at different locations experience distinct stress paths. When taking different stress paths as a variable, the cohesion and internal friction angle of rocks were calculated to accurately describe the evolution of the strength parameters of surrounding rocks in deep excavation. First, according to the 3D linear failure criterion established by Feng et al. (2020b), Eqs. (10) and (11) can be defined:

$$\left[\sqrt{1-b+sb^2}+t\left(1-\sqrt{1-b+b^2}\right)\sin\varphi\right](\sigma_1-\sigma_3) = (\sigma_1+\sigma_3)\sin\varphi+2c\cos\varphi \tag{10}$$

$$b=\frac{\sigma_2-\sigma_3}{\sigma_1-\sigma_3} \tag{11}$$

where b represents the intermediate principal stress coefficient, and s and t are the material parameters. Fig. 7 and Table 2 show the peak strength of Shuangjiangkou granite under true triaxial compression and different stress states. The corresponding $s=0.95$ and $t=0.9$ can be obtained according to the 3D failure criterion.

The stress (σ_{cd}) corresponding to the first volumetric strain inflection point of cyclic loading and unloading was used to calculate the initial internal friction angle (φ_0). It was assumed that the φ of the rock sample at σ_{cd} of each cycle was the same. Since cyclic loading and unloading tests under different σ_3 conditions were not performed in this study, σ_{cd} in the loading test was similar to σ_{cd} in the first cycle of the cyclic loading and unloading test. Therefore, σ_{cd} in the loading test under different confining pressures was used to calculate φ_0 (Table 2). Then, s and t were maintained, and c was calculated from σ_{cd} and φ in each cycle, as expressed in Eq. (12):

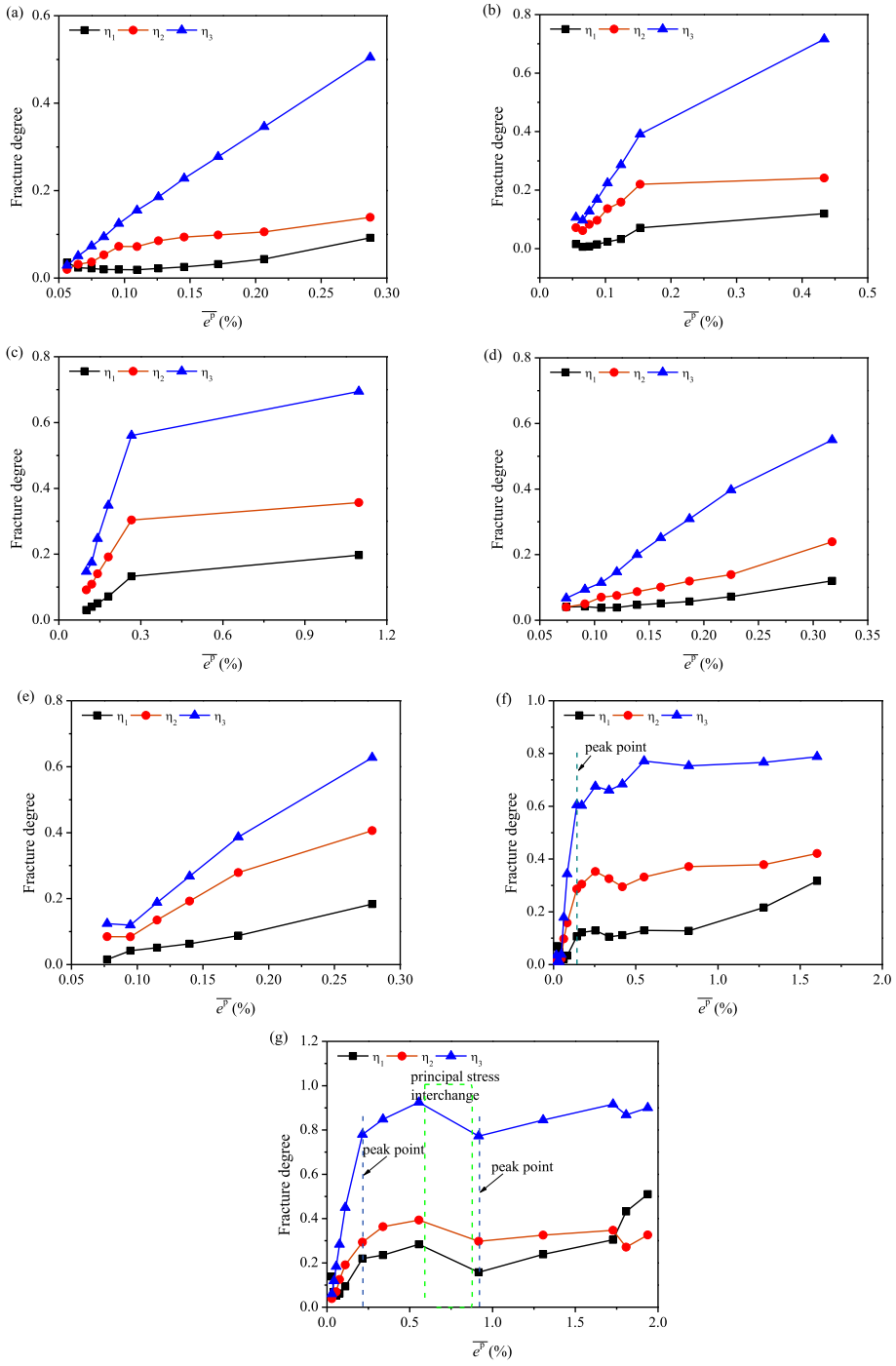

Fig. 6. Evolution of the fracture degrees of Shuangjiangkou granite in the three principal stress directions with equivalent crack strain under different stress paths: (a) SKJ-1-1, (b) SKJ-1-2, (c) SKJ-1-3, (d) SKJ-1-4, (e) SKJ-1-5, (f) SKJ-1-6, and (g) SKJ-1-7.

$$c = \frac{\left[\sqrt{1-b+sb^2}+t\left(1-\sqrt{1-b+b^2}\right)\sin\varphi_0\right](\sigma_{cd}-\sigma_3)-(\sigma_{cd}+\sigma_3)\sin\varphi_0}{2\cos\varphi_0} \tag{12}$$

where the initial φ_0 of Shuangjiangkou granite was 50.6°. The σ_{cd} under each cycle is shown in Fig. 8.

The value of c for each cycle can be calculated by Eq. (12), and then using the peak stress and c of each cycle, the values of φ for each cycle can be obtained through Eqs. (13) and (14):

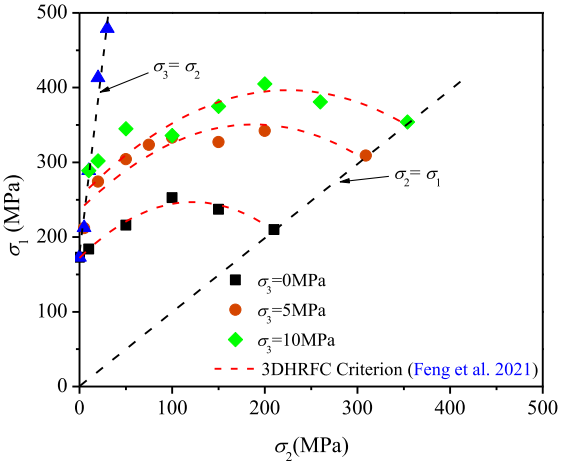

Fig. 7. Strength of Shuangjiangkou granite under true triaxial compression.

Table 2
The σ_{cd} in the loading test under different σ_3 conditions.

σ_3 (MPa)	σ_2 (MPa)	σ_{cd} (MPa)
0	0	107
5	5	165
10	10	213
20	20	283
30	30	347

$$\varphi = \sin^{-1}\frac{\sqrt{1-b+sb^2}(\sigma_1-\sigma_3)}{\sqrt{a^2+4c^2}} - \tan^{-1}\left(\frac{2c}{a}\right) \tag{13}$$

$$a = (\sigma_1+\sigma_3) - t\left(1-\sqrt{1-b+b^2}\right)(\sigma_1-\sigma_3) \tag{14}$$

4.2. Cohesion and internal friction angle

Fig. 9 shows the evolution of the cohesion and internal friction angle with the equivalent crack strain of Shuangjiangkou granite during cyclic loading and unloading for different stress paths. It can be found that the evolution of the cohesion and internal friction angle exhibited the same trend. The value of c decreased with the increase in equivalent crack strain, which is mainly due to the increase in the stress difference during cyclic loading and unloading and led to the continuous increase of the equivalent crack strain, the decay of the mechanical properties of materials around the crack, and a gradual decrease in c. For different stress paths, the internal friction angle φ increased with increasing equivalent crack strain, which was affected by the friction coefficient, and its size was related to the roughness of the potential sliding surface. With the increase in the equivalent crack strain, many microcracks were generated, and thus the friction coefficient of the rock increased, resulting in an increased φ. It can thus be concluded that, although rocks experience different stress paths during the excavation of deep hard rock, the adjustments of the cohesion and internal friction angle are basically the same. These trends are summarized as the increase in rock friction strength accompanied by the loss of cohesion for different stress paths, in which the change in stress direction is not taken into account. In the CLU–TSI test, when the σ_1 and σ_2 directions were interchanged, the value of φ slightly decreased and c significantly increased. After the principal stress direction interchanged, the development position of the crack changed, the number of cracks in the new fracture area decreased, the mechanical properties of surrounding rocks increased, and thus cohesion increased.

5. Discussion

5.1. Effect of stress path on rock fracture difference

To clarify the effect of the stress path on rock fracture, it is necessary to quantify the different stress paths. As shown in Fig. 10, in octahedral stress space, different stress paths have unique motion trajectories. Therefore, the deflection radian value β_R was used to characterize the stress path coefficient that represents the movement direction from the stress state to the failure line at a certain point, as expressed in Eqs. (15)–(21):

$$\beta_R = \arctan\left(\frac{\Delta q}{\Delta p}\right) \tag{15}$$

$$\Delta q = q_1 - q_0 \tag{16}$$

$$\Delta p = p_1 - p_0 \tag{17}$$

$$p_0 = \frac{1}{3}\left(\sigma_1^0+\sigma_2^0+\sigma_3^0\right) \tag{18}$$

$$p_1 = \frac{1}{3}(\sigma_1+\sigma_2+\sigma_3) \tag{19}$$

$$q_0 = \frac{1}{\sqrt{2}}\left[\left(\sigma_1^0-\sigma_2^0\right)^2+\left(\sigma_2^0-\sigma_3^0\right)^2+\left(\sigma_3^0-\sigma_1^0\right)^2\right]^{\frac{1}{2}} \tag{20}$$

$$q_1 = \frac{1}{\sqrt{2}}\left[(\sigma_1-\sigma_2)^2+(\sigma_2-\sigma_3)^2+(\sigma_3-\sigma_1)^2\right]^{\frac{1}{2}} \tag{21}$$

where β_R is the stress path coefficient; q is the generalized shear stress; p is the average stress; and the superscripts 0 and 1 are the initial and final stress states, respectively.

The development of rock fracture occurred mainly in the σ_2–σ_3 plane. To compare the fractures differences for the different stress

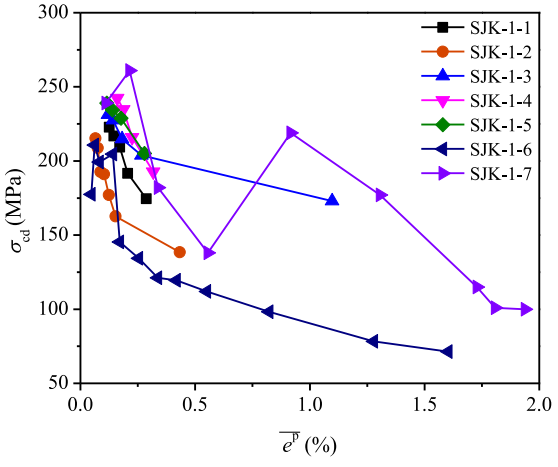

Fig. 8. The σ_{cd} of Shuangjiangkou granite for different stress paths during cyclic loading and unloading.

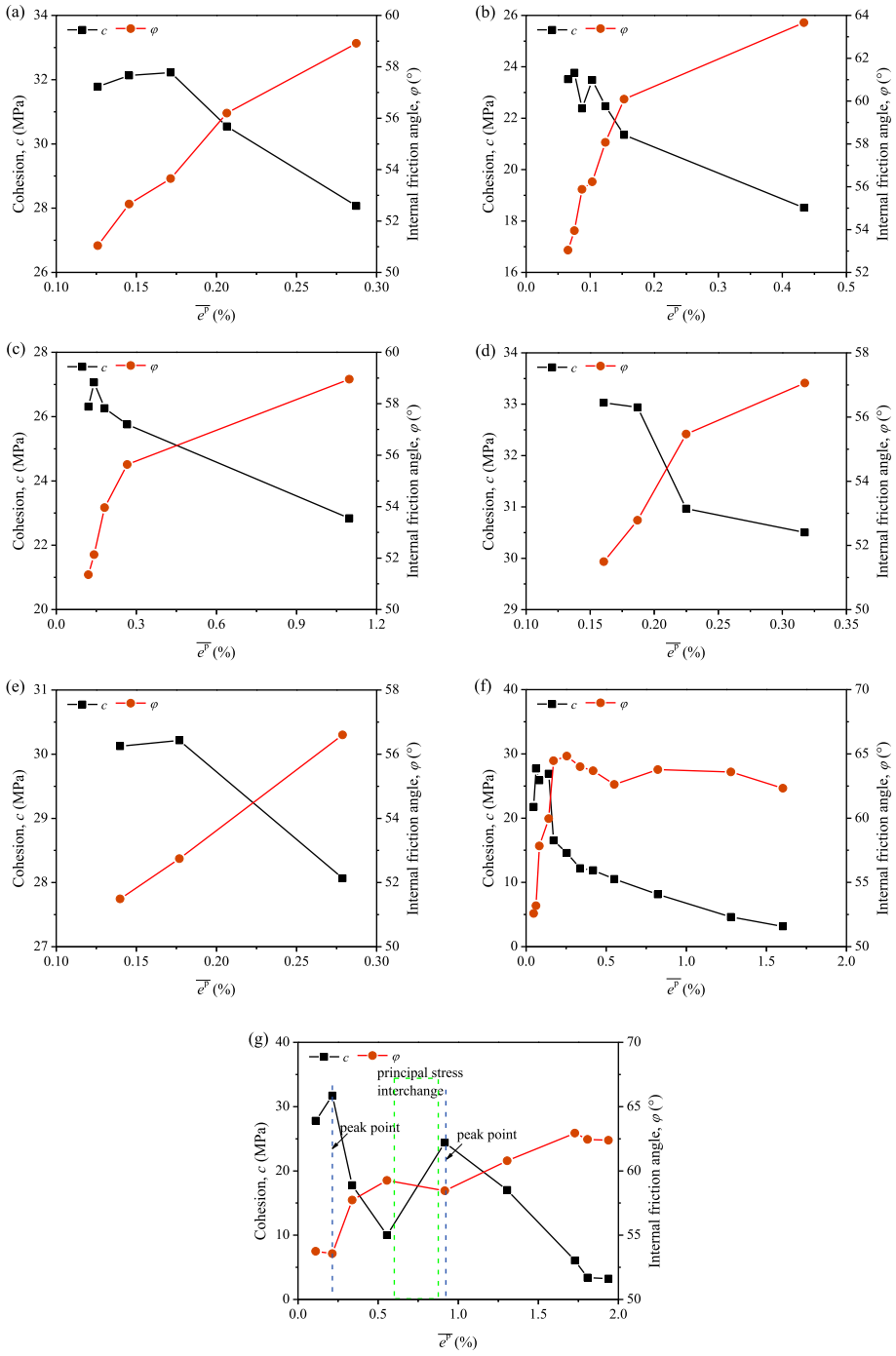

Fig. 9. Evolution of the cohesion and internal friction angle with the equivalent crack strain of Shuangjiangkou granite under different stress paths during cyclic loading and unloading: (a) SKJ-1-1, (b) SKJ-1-2, (c) SKJ-1-3, (d) SKJ-1-4, (e) SKJ-1-5, (f) SKJ-1-6, and (g) SKJ-1-7.

paths in the σ_2 and σ_3 directions, the fracture degree difference coefficient λ is defined as Eq. (22):

$$\lambda = \frac{\eta_3 - \eta_2}{\eta_3} \tag{22}$$

To quantify the effects of different stress paths on rock fracture differences, data for the stress path coefficient and fracture degree difference coefficient were fitted. The fracture degree difference coefficient of rocks under different stress paths had an exponential relationship with the stress path coefficient, as expressed in Eq. (23) and shown in Fig. 11.

$$\lambda = -0.05773\exp(\beta_R) + 0.71325 \tag{23}$$

It can thus be concluded that the effect of the stress path on the fracture difference of rock cannot be neglected in deep excavation. However, the stress path used here included only the engineering excavation stress path proposed in this paper. For other complex

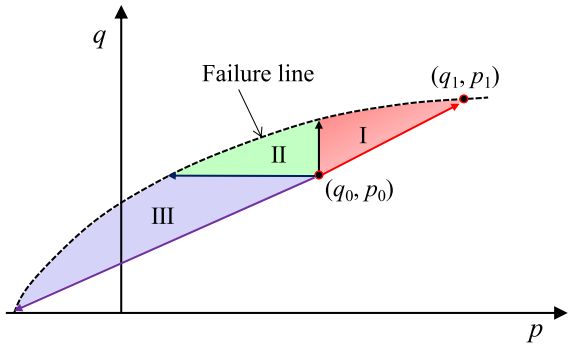

Fig. 10. Schematic diagram of different stress paths in octahedral stress space.

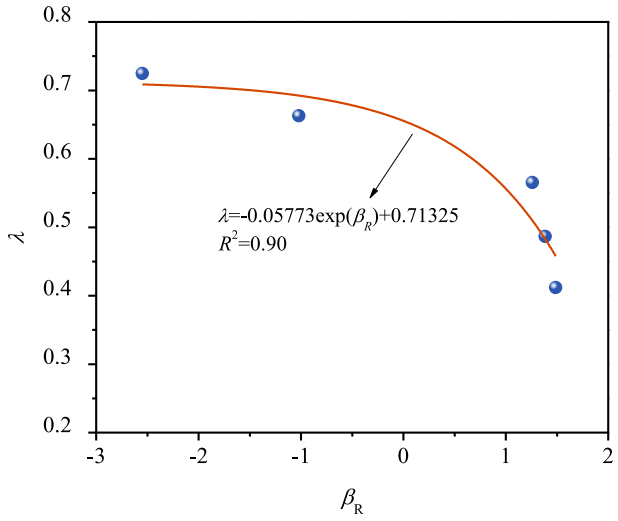

Fig. 11. Relationship between the fracture difference and stress path coefficients of Shuangjiangkou granite under different stress paths.

stress paths and principal stress direction interchanges, further research is still needed.

5.2. Effect of stress path on rock cohesion and internal friction angle

According to the above analysis, the φ increased and c decreased with increasing equivalent crack strain. To further compare the evolution of the cohesion and internal friction angle for different stress paths, normalization was used to characterize the development of the damage degree:

Table 3
Linear fitting parameters of the cohesion and internal friction angle for different stress paths.

Strength parameter	Stress path	k	b	R^2
c	SKJ-1-1	−5.9662	34.334	0.8839
	SKJ-1-2	−5.1278	23.483	0.9055
	SKJ-1-3	−3.8438	26.651	0.9561
	SKJ-1-4	−4.1644	34.398	0.8004
	SKJ-1-5	−3.2562	31.428	0.9138
φ	SKJ-1-1	11.118	48.185	0.9727
	SKJ-1-2	9.6251	54.889	0.7938
	SKJ-1-3	6.5655	52.691	0.8122
	SKJ-1-4	8.4864	49.028	0.8984
	SKJ-1-5	7.465	49.117	0.9995

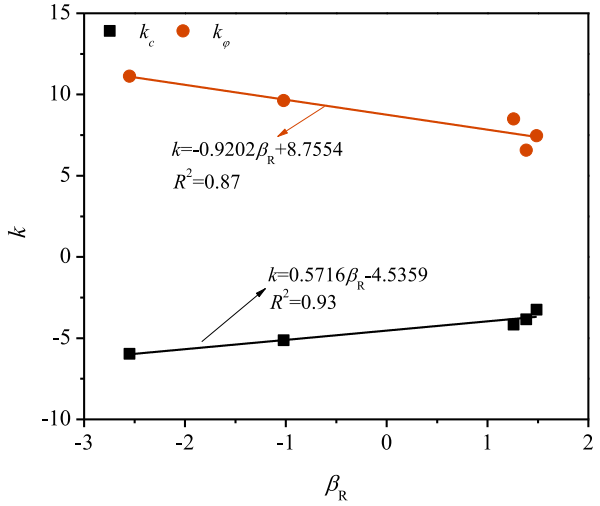

Fig. 12. Relationships between the slopes of c and φ and the stress path coefficient of Shuangjiangkou granite during cyclic loading and unloading for different stress paths.

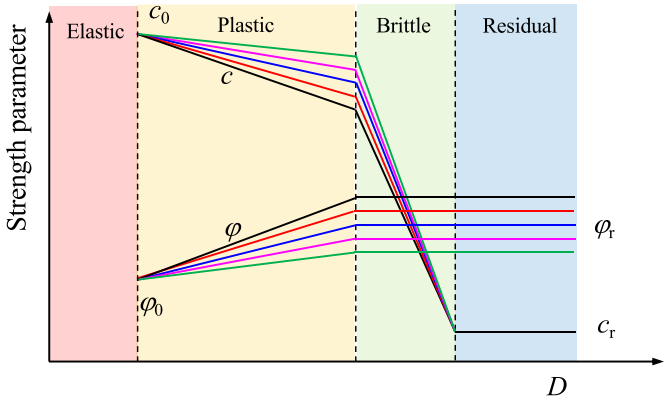

Fig. 13. Evolution of c and φ of Shuangjiangkou granite under different stress paths.

$$D = \frac{\overline{e^{\mathrm{p}}} - \overline{e^{\mathrm{p}}_{\min}}}{\overline{e^{\mathrm{p}}_{\max}} - \overline{e^{\mathrm{p}}_{\min}}} \quad (D \in (0,1)) \tag{24}$$

The relationships between the damage degree D and c and φ for different stress paths were fitted by linear functions, as expressed in Eqs. (25) and (26):

$$c = k_c D + b_c \tag{25}$$

$$\varphi = k_\varphi D + b_\varphi \tag{26}$$

where k_c and k_φ represent the changing speeds of c and φ with the increase in D, and b_c and b_φ are the corresponding intercepts. The results are shown in Table 3.

As shown in Fig. 12, with the increase in the stress path coefficient, the degrees of c weakening and φ strengthening decreased, which can be described by linear relationships with fitting coefficient larger than 0.85. Therefore, the change in the stress path affected the changes degrees of the cohesion and internal friction angle.

Due to the stress control mode adopted in the CLU–TLU test, the rock sample fractured rapidly when the stress reached peak strength, which was consistent with brittle failure. Therefore, the

instantaneous stress drop (ISD) fracture mechanism proposed by Feng et al. (2021) was used to explain the post-peak stage, in which the sudden loss of cohesion was caused by the opening or penetration of macrocracks. Additionally, due to the short duration of the process, the friction strength was almost unchanged. When the initial values of the cohesion and internal friction angle were consistent, the evolution for different stress paths is shown in Fig. 13. Specifically, the value of c decreased and φ increased before the peak; however, different stress paths led to different evolution slopes of c and φ. At the post-peak stage, the value of c decreased to the residual stage and remained unchanged, and φ remained basically unchanged due to the penetration of macrocracks (Fig. 13).

5.3. Effects of principal stress direction interchange on the stability of deep excavation

Deep hard rock engineering operations are prone to brittle disasters, such as rockbursts, spalling and collapse. Accurately obtaining the evolution of mechanical parameters of surrounding rocks after deep hard rock excavation may provide a research basis for guaranteeing the construction safety of deep engineering projects.

After underground excavation, the surrounding rock undergoes different stress paths. The evolution of the strength parameters shows the weakening of cohesion and the strengthening of the internal friction angle. However, due to the change in stress direction, the direction of crack development changes, the cohesion increases, the internal friction angle decreases, and the mechanical properties improve, as shown in Figs. 4g, 5g and 6g and 9g, respectively. Therefore, when considering the optimization of the support of surrounding rocks, the strength and mechanical parameters of the support should be determined according to the adjustments of the stress magnitude and direction to ensure the safety and stability of deep engineering projects.

6. Conclusions

In this study, a new true triaxial cyclic loading and unloading test method under different stress paths was proposed to quantify the evolution of mechanical parameters of surrounding rocks. The main conclusions are drawn as follows:

(1) Under true triaxial conditions, the elastic strain increment ratios in the σ_3 direction is larger than that in the σ_2 direction, and the rock fractures are parallel to the σ_2 direction. The smaller the value of σ_3 or the greater the stress difference between σ_2 and σ_3 when rocks failed, the larger the rock failure angle is.

(2) Under CLU–TLU, with the increase in the equivalent crack strain, the deformation modulus and cohesion of rocks gradually decrease, while the elastic strain increment ratios, the fracture degree coefficients and the internal friction angle gradually increase, showing that the rock gradually deteriorates.

(3) Under CLU–TSI, the direction of crack development changes, both the deformation modulus and cohesion of rocks increase, while the elastic strain increment ratios, the fracture degree coefficients in the three principal stress directions and the internal friction angle decreases, showing the characteristics of rock strengthening

(4) The stress path coefficient and the rock fracture degree coefficient are exponentially related. Different stress paths lead to different cohesion weakening and internal friction angle strengthening trends, which can be described using a linear functional relationship.

(5) The stress path influences the evolution of the mechanical parameters of rocks. When establishing a constitutive model of rock, the effect of the stress path should be considered, and when considering the optimization of deep rock support, the strength and related parameters of support should be determined according to adjustments of the magnitude and direction of stress to ensure the safety and stability of deep engineering projects.

Declaration of competing interest

The authors declare that they have no known competing financial interests or personal relationships that could have appeared to influence the work reported in this paper.

Acknowledgments

The authors gratefully acknowledge the financial support from the National Natural Science Foundation of China (Grant Nos. 51839003 and 42207221). The authors also would like to thank Mr. Benguo He, Mr. Zhaofeng Wang, Mr. Yaohui Gao, Mr. Jianwei Lu, and Ms. Xinyue Wang for their kind assistance.

References

Andersson, J.C., Martin, C.D., Stille, H., 2009. The Äspö pillar stability experiment: part II-rock mass response to coupled excavation-induced and thermal-induced stresses. Int. J. Rock Mech. Min. 46 (5), 879–895.

Bai, Q., Tibbo, M., Nasseri, M.H.B., Young, R.P., 2019. True triaxial experimental investigation of rock response around the mine-by tunnel under an in situ 3D stress path. Rock Mech. Rock Eng. 52, 3971–3986.

Basarir, H., Oge, I.F., Aydin, O., 2015. Prediction of the stresses around main and tail gates during top coal caving by 3D numerical analysis. Int. J. Rock Mech. Min. 76, 88–97.

Cai, M., Kaiser, P.K., Tasaka, Y., Maejima, T., Morioka, H., Minami, M., 2004. Generalized crack initiation and crack damage stress thresholds of brittle rock masses near underground excavations. Int. J. Rock Mech. Min. 41 (5), 833–847.

Cai, W.Q., Zhu, H.H., Liang, W.H., 2022. Three-dimensional stress rotation and control mechanism of deep tunneling incorporating generalized Zhang–Zhu strength-based forward analysis. Eng. Geol. 308, 106806s.

Cai, W.Q., Zhu, H.H., Liang, W.H., Wang, X.J., Su, C.L., Wei, X.Y., 2023. A post-peak dilatancy model for soft rock and its application in deep tunnel excavation. J. Rock Mech. Geotech. 15 (3), 683–701.

Chen, C.N., Huang, W.Y., 2007. Investigation of tunnel stress path during face advancement. J. Mech. 23, 451–458.

Chen, J., Jiang, D.Y., Ren, S., Yang, C.H., 2016. Comparison of the characteristics of rock salt exposed to loading and unloading of confining pressures. Acta Geotech 11 (1), 221–230.

Diederichs, M.S., 2007. The 2003 Canadian geotechnical colloquium: mechanistic interpretation and practical application of damage and spalling prediction criteria for deep tunnelling. Can. Geotech. J. 44 (9), 1082–1116.

Diederichs, M.S., Kaiser, P.K., Eberhardt, E., 2004. Damage initiation and propagation in hard rock during tunnelling and the influence of near face stress rotation. Int. J. Rock Mech. Min. 41 (5), 785–812.

Duan, K., Ji, Y.L., Wu, W., Kwok, C.Y., 2019. Unloading-induced failure of brittle rock and implications for excavation-induced strain burst. Tunn. Undergr. Space Technol. 84, 495–506.

Duan, S.Q., Jiang, Q., Liu, G.F., Xiong, J.C., Li, M.Y., 2021b. An insight into the excavation-induced stress paths on mechanical response of weak interlayer zone in underground cavern under high geostress. Rock Mech. Rock Eng. 54 (3), 1331–1354.

Duan, M., Jiang, C., Yin, W., Yang, K., Liu, Q., 2021a. Experimental study on mechanical and damage characteristics of coal under true triaxial cyclic disturbance. Eng. Geol. 295, 106445.

Eberhardt, E., 2001. Numerical modelling of three-dimension stress rotation ahead of an advancing tunnel face. Int. J. Rock Mech. Min. 38, 499–518.

Feng, X.T., 2017. Rockburst: Mechanisms, Monitoring, Warning, and Mitigation. Butterworth-Heinemann.

Feng, X.T., Gao, Y.H., Zhang, X.W., Wang, Z.F., Han, Q., 2020a. Evolution of the mechanical and strength parameters of hard rocks in the true triaxial cyclic loading and unloading tests. Int. J. Rock Mech. Min. 131 (6), 104349.

Feng, X.T., Haimson, B., Li, X.C., Chang, C.D., Ma, X.D., Zhang, X., Ingraham, M., Suzuki, K., 2019. ISRM suggested method: determining deformation and failure characteristics of rocks subjected to true triaxial compression. Rock Mech. Rock Eng. 52, 2011–2020.

Feng, X.T., Kong, R., Yang, C.X., Zhang, X.W., Wang, Z.F., Han, Q., Wang, G., 2020b. A three-dimensional failure criterion for hard rocks under true triaxial compression. Rock Mech. Rock Eng. 53, 103–111.
Feng, X.T., Wang, Z., Zhou, Y., Yang, C., Kong, R., 2021. Modelling three-dimensional stress-dependent failure of hard rocks. Acta Geotech 16, 1–31.
Feng, X.T., Xu, H., Yang, C.X., Zhang, X.W., Gao, Y.H., 2020c. Influence of loading and unloading stress paths on the deformation and failure features of jinping marble under true triaxial compression. Rock Mech. Rock Eng. 53, 3287–3301.
Feng, X.T., Yang, C.X., Kong, R., Zhao, J., Zhou, Y.Y., Yao, Z.B., Hu, L., 2022. Excavation-induced deep hard rock fracturing: methodology and applications. J. Rock Mech. Geotech. 14 (1), 1–34.
Feng, X.T., Zhang, X., Kong, R., Wang, G., 2016. A novel Mogi type true triaxial testing apparatus and its use to obtain complete stress–strain curves of hard rocks. Rock Mech. Rock Eng. 49, 1649–1662.
Gu, L.J., Feng, X.T., Kong, R., Yang, C.X., 2023. Effect of principal stress direction interchange on the failure characteristics of hard rock. Int. J. Rock Mech. Min. 164, 105365.
Gu, L.J., Feng, X.T., Kong, R., Yang, C.X., Han, Q., Xia, Y.L., 2022. Excavation stress path induced fracturing mechanism of hard rock in deep tunnel. Rock Mech. Rock Eng. 56 (3), 1779–1806.
Hajiabdolmajid, V., Kaiser, P.K., Martin, C.D., 2002. Modelling brittle failure of rock. Int. J. Rock Mech. Min. 39 (6), 731–741.
He, M.C., Li, J.Y., Liu, D.Q., Li, K., Ren, F.Q., 2021. A novel true triaxial apparatus for simulating strain bursts under high stress. Rock Mech. Rock Eng. 54, 759–775.
Heap, M.J., Faulkner, D.R., 2008. Quantifying the evolution of static elastic properties as crystalline rock approaches failure. Int. J. Rock Mech. Min. 45 (4), 564–573.
Hoek, E., Brown, E.T., 1997. Practical estimates of rock mass strength. Int. J. Rock Mech. Min. 34 (8), 1165–1186.
Huang, R.Q., Huang, D., 2014. Evolution of rock cracks under unloading condition. Rock Mech. Rock Eng. 47 (2), 453–466.
Huang, R.Q., Wang, X.N., Chan, L.S., 2001. Triaxial unloading test of rocks and its implication for rock burst. Bull. Eng. Geol. Environ. 60, 37–41.
Jiang, B.Y., Gu, S.T., Wang, L.G., Zhang, G.C., Li, W.S., 2019. Strainburst process of marble in tunnel-excavation-induced stress path considering intermediate principal stress. J. Cent. South. Univ. 26 (4), 984–999.
Jiang, C., Wang, L., Ding, K., Wang, S., Ren, B., Guo, J.X., 2023. Experimental study on mechanical and damage evolution characteristics of coal during true triaxial cyclic loading and unloading. Materials 16 (6), 2384.
Kaiser, P.K., 2005. Tunnel stability in highly stressed, brittle ground—rock mechanics considerations for Alpine tunnelling. Geologie und Geotechnik der Basistunnels am Gotthard und am Lötschberg. 2005, 183–202.
Kaiser, P.K., Yazici, S., Maloney, S., 2001. Mining-induced stress change and consequences of stress path on excavation stability. a case study 38, 167–180.
Kong, R., Tuncay, E., Ulusay, R., Zhang, X., Feng, X.-T., 2021. An experimental investigation on stress-induced cracking mechanisms of a volcanic rock. Eng. Geol. 280, 105934.
Kovari, K., Tisa, A., Einstein, H.H., Franklin, J.A., 1983. Suggested methods for determining the strength of rock materials in triaxial compression: revised version. Int. J. Rock Mech. Min. 20 (6), 283–290.
Lee, H., Haimson, B.C., 2011. True triaxial strength, deformability, and brittle failure of granodiorite from the San Andreas Fault Observatory at Depth. Int. J. Rock Mech. Min. 48 (7), 1199–1207.
Li, X.B., Du, K., Li, D.Y., 2015. True triaxial strength and failure modes of cubic rock specimens with unloading the minor principal stress. Rock Mech. Rock Eng. 48, 2185–2196.
Li, J.H., Sheng, Q., Zhu, Z.Q., Leng, X.L., Niu, L.M., Liu, S.W., 2017b. Analysis of stress path and failure mode of sur rounding rock during Mine-by test tunnel excavation. Chin. J. Rock Mech. Eng. 36, 821–830, 04.
Li, D., Sun, Z., Xie, T., Li, X., Ranjith, P.G., 2017a. Energy evolution characteristics of hard rock during triaxial failure with different loading and unloading paths. Eng. Geol. 228, 270–283.
Li, Z.K., Zhou, Z., Tang, X.F., Liao, C.G., Hou, D.Q., Xing, X.L., Zhang, Z.Z., Liu, Z.G., Chen, Q.H., 2009. Stability analysis and considerations of underground powerhouse caverns group of Jinping I hydropower station. Chin. J. Geotech. Eng. 28 (11), 2167–2175 (in Chinese).
Liang, Y.P., Li, Q.M., Gu, Y.L., Zou, Q.L., 2017. Mechanical and acoustic emission characteristics of rock: effect of loading and unloading confining pressure at the postpeak stage. J. Nat. Gas Sci. Eng. 44 (5), 54–64.
Liu, H., Pei, J., Liu, J., Xiao, M.L., Zhuo, Li, Xie, H.Q., 2023b. Influence of volume compression on the unloading deformation behavior of red sandstone under damage-controlled cyclic triaxial loading. J. Rock Mech. Geotech. 15 (5), 1200–1212.
Liu, C., Zhao, G., Xu, W., Meng, X.R., Liu, Z.X., Cheng, X., Lin, G., 2023a. Experimental study on failure characteristics of single-sided unloading rock under different intermediate principal stress conditions. Int. J. Min. Sci. Technol. 33 (3), 275–287.
Martin, C.D., Chandler, N.A., 1994. The progressive fracture of Lac du Bonnet granite. Int. J. Rock Mech. Min. Sci. Geomech. Abstr. 31 (6), 643–659.
Martin, C.D., Christiansson, R., 2009. Estimating the potential for spalling around a deep nuclear waste repository in crystalline rock. Int. J. Rock Mech. Min. Sci. 46 (2), 219–228.
Meng, Q.B., Liu, J.F., Ren, L., Pu, H., Chen, Y.L., 2021. Experimental study on rock strength and deformation characteristics under triaxial cyclic loading and unloading conditions. Rock Mech. Rock Eng. 54 (2), 777–797.
Momeni, A., Karakus, M., Khanlari, G.R., Heidari, M., 2015. Effects of cyclic loading on the mechanical properties of a granite. Int. J. Rock Mech. Min. 77, 89–96.
Ortlepp, W.D., 2005. RaSiM comes of age – a review of the contribution to the understanding and control of mine rockburst. In: Proceeding of the 6th International Symposium on Rockburst and Seismicity in Mines. Australian Centre for Geomechanics, pp. 3–20.
Poinard, C., Malecot, Y., Daudeville, L., 2010. Damage of concrete in a very high stress state: experimental investigation. Mater. Struct. 43 (1–2), 15–29.
Qiu, S.L., Feng, X.T., Xiao, J.Q., Zhang, C.Q., 2014. An experimental study on the pre-peak unloading damage evolution of marble. Rock Mech. Rock Eng. 47, 401–419.
Renani, H.R., Martin, C.D., 2018. Cohesion degradation and friction mobilization in brittle failure of rocks. Int. J. Rock Mech. Min. 106, 1–13.
Rojat, F., Labiouse, V., Kaiser, P.K., Descoeudres, F., 2009. Brittle rock failure in the Steg lateral adit of the Lötschberg base tunnel. Rock Mech. Rock Eng. 42 (2), 341–359.
Sun, B., Zhu, Z.D., Shi, C., Luo, Z.H., 2017. Dynamic mechanical behavior and fatigue damage evolution of sandstone under cyclic loading. Int. J. Rock Mech. Min. 94, 82–89.
Taheri, A., Royle, A., Yang, Z., Zhao, Y., 2016. Study on variations of peak strength of a sandstone during cyclic loading. Geomech. Geophys. Geo-Energy Geo-Resour. 2, 1–10.
Wang, C.L., Gao, A.S., Shi, F., Hou, X.L., Ni, P.P., Ba, D.Y., 2019a. Three-dimensional reconstruction and growth factor model for rock cracks under uniaxial cyclic loading/unloading by X-ray CT. Geotech. Test J. 42 (1), 117–135.
Wang, D.H., He, S.H., Liu, X.B., Li, C.H., Zhang, J.W., 2019b. A modified method for determining the overburden pressure above shallow tunnels considering the distribution of the principal stress rotation and the partially mobilized arching effect. Chin. J. Rock Mech. Eng. 38, 1284–1296, 06.
Wang, Z.H., Wang, J.C., Yang, S.L., 2018. An ultrasonic based method for longwall top-coal cavability assessment. Int. J. Rock Mech. Min. 112, 209–225.
Xiao, J.Q., Ding, D.X., Jiang, F.L., Xu, G., 2010. Fatigue damage variable and evolution of rock subjected to cyclic loading. Int. J. Rock Mech. Min. 47, 461–468.
Xu, H., Feng, X.T., Yang, C.X., Zhang, X.W., Zhou, Y.Y., Wang, Z.F., 2019. Influence of initial stresses and unloading rates on the deformation and failure mechanism of Jinping marble under true triaxial compression. Int. J. Rock Mech. Min. 117, 90–104.
Yin, P.F., Yang, S.Q., Gao, F., Tian, W.L., 2023. Experiment and DEM simulation study on mechanical behaviors of shale under triaxial cyclic loading and unloading conditions. Geomech. Geophy. 9 (1), 10.
Zhang, C.Q., Feng, X.T., Hui, Z., 2012. Estimation of in situ stress along deep tunnels buried in complex geological conditions. Int. J. Rock Mech. Min. 52, 139–162.
Zhang, L.C., Meng, Y., Wang, F.Z., Zhang, Z.Q., Su, P.G., 2021. Energy evolution analysis and failure criteria for rock under different stress paths. Acta Geotech 16 (2), 569–580.
Zhao, J., Feng, X.T., Guo, H.S., Hu, Y., Chen, G., Yang, C.X., 2022. Time-dependent failure characteristics of excavated rock masses in deep buried engineering: a field case and experimental study. Bull. Eng. Geol. Environ. 81, 520.
Zhao, Y., Wang, Y., Wang, W., Wan, W., Tang, J.Z., 2017. Modeling of non-linear rheological behavior of hard rock using triaxial rheological experiment. Int. J. Rock Mech. Min. 93, 66–75.
Zhou, Y.Q., Sheng, Q., Li, N.N., Fu, X.D., 2022. The dynamic mechanical properties of a hard rock under true triaxial damage-controlled dynamic cyclic loading with different loading rates: a case study. Rock Mech. Rock Eng. 55, 1–22.
Zhu, C., Karakus, M., He, M.C., Meng, Q.X., Shang, J.L., Wang, Y., Yin, Q., 2022. Volumetric deformation and damage evolution of Tibet interbedded skarn under multistage constant-amplitude-cyclic loading. Int. J. Rock Mech. Min. 152, 105066.

Prof. Xia-Ting Feng received his PhD degree at Northeastern University of Technology (now Northeastern University since 1993), China in 1992 and then took the position of lecturer, associate professor and professor at the same university. He joined Institute of Rock and Soil Mechanics, Chinese Academy of Sciences (CAS) in 1998 as a Professor of Hundred Talent Program of the CAS and as Deputy Director in Charge and Director in 2001–2005. He has worked as Director of State Key Laboratory of Geomechanics and Geotechnical Engineering since 2007. He works at Northeastern University, China as a Vice President since September 2017. In February 2021, he became president of Northeastern University. He is President of Federation of International Geo-engineering Societies–FedIGS, President of International Society for Rock Mechanics (ISRM) Commission on Design Methodology, member of ISRM Commission on Testing Methods, and President of Chinese Society for Rock Mechanics and Engineering (CSRME). He was the past President of ISRM 2011–2015. He is also Editor-in-Chief of *Journal of Rock Mechanics and Geotechnical Engineering* (JRMGE), and Associate Editor-in-Chief of *Chinese Journal of Theoretical and Applied Mechanics*. He is member of Editorial Board of *Rock Mechanics and Rock Engineering*. His research interests cover rock mechanics for deep rock engineering. He published more than 200 technical papers and the English books "*Rock engineering design*" and "*Rock engineering risk*" with Professor John Hudson. He has edited five volumes of the book "*Rock mechanics and rock engineering*" (CRC Press) and the book "*Rockburst*" (Elsevier).